Relaxation processes following 1s photoionization and Auger decay in Ne₂

K. Kreidi,[1,2] T. Jahnke,[1] Th. Weber,[3] T. Havermeier,[1] X. Liu,[4] Y. Morisita,[5] S. Schössler,[1] L. Ph. H. Schmidt,[1]
M. Schöffler,[1] M. Odenweller,[1] N. Neumann,[1] L. Foucar,[1] J. Titze,[1] B. Ulrich,[1] F. Sturm,[1] C. Stuck,[1] R. Wallauer,[1]
S. Voss,[1] I. Lauter,[1] H. K. Kim,[1] M. Rudloff,[1] H. Fukuzawa,[4] G. Prümper,[4] N. Saito,[5] K. Ueda,[4] A. Czasch,[1]
O. Jagutzki,[1] H. Schmidt-Böcking,[1] S. Stoychev,[6] Ph. V. Demekhin,[6,7] and R. Dörner[1,*]

[1]*Institut für Kernphysik, J. W. Goethe-Universität, Max-von-Laue-Straße 1, 60438 Frankfurt, Germany*
[2]*DESY, Notkestraße 85, 22607 Hamburg, Germany*
[3]*Lawrence Berkeley National Laboratory, Berkeley, California 94720, USA*
[4]*Institute of Multidisciplinary Research for Advanced Materials, Tohoku University, Sendai 980-8577, Japan*
[5]*National Metrology Institute of Japan, AIST, Tsukuba 305-8568, Japan*
[6]*Theoretische Chemie, Universität Heidelberg, Im Neuenheimer Feld 229, 69120 Heidelberg, Germany*
[7]*Institut fur Physik, Experimental-Physik IV, Universität Kassel, Heinrich-Plett-Straße 40, 34132 Kassel, Germany*

We used cold target recoil ion momentum spectroscopy for a comprehensive study of the decay of a neon dimer (Ne₂) after removal of a 1s electron from one of the atoms of the dimer. Multiple decay pathways are found and identified, mostly being connected to different types of interatomic Coulombic decay (ICD) such as the "direct" ICD which happens via the transfer of a virtual photon, the "exchange" ICD via an electron transfer and the electron transfer mediated decay. A quantitative theoretical analysis of these decay processes can be found in the preceding paper by Demekhin *et al.* [Phys. Rev. A **78**, 043421 (2008)], as well as in Stoychev *et al.* [J. Chem. Phys. **129**, 074307 (2008)].

PACS number(s): 33.80.Eh, 33.15.Dj, 33.15.Ry, 34.70.+e

I. INTRODUCTION

In the pioneering work by Cederbaum *et al.* a class of decay processes that occurs only for loosely bound compounds of matter was proposed in 1997 [1]. If an atom is excited and ionized in an inner valence shell, in many cases it cannot deexcite via Auger decay, i.e., with the emission of an electron, as the excitation energy is not sufficient to emit even the most loosely bound electron from that ion. In such a case the ion will undergo radiative decay. Cederbaum *et al.*, however, demonstrated theoretically that this situation changes as soon as the ion is located in the vicinity of another atom. The energy that is gained from the transition of an outer shell electron to the inner valence vacancy is usually sufficient to ionize a neutral atomic neighbor. Furthermore, the competing process of radiative decay is very slow compared to typical electronic decays involving electron emission making this two center decay the dominant relaxation pathway for ions that reside in a chemical environment. Cederbaum predicted that this process, termed interatomic Coulombic decay (ICD), will occur in all loosely bound matter as van der Waals clusters or hydrogen bond systems. It took almost ten years before these predictions were confirmed experimentally: Marburger *et al.* found first indications for ICD in large neon clusters employing electron spectroscopy [2] and Jahnke *et al.* unambiguously demonstrated the existence of ICD in a neon dimer after 2s ionization by measuring all particles from the decay in coincidence using a cold target recoil ion momentum spectroscopy (COLTRIMS) setup [3]. Many further studies demonstrated that ICD is very general: ICD was found for resonant excitation of atoms [4,5]

[termed "resonant ICD" (RICD)], as well as for the case of population of satellite states in shakeup excitation [6] [termed "shakeup-induced ICD" (SICD)].

Earlier theoretical work by Santra *et al.* showed that ICD will occur after innershell ionization of Ne₂ as well [7]. In this case, generally, ICD happens as a terminal step after an atomic Auger cascade at the initially excited atom. While in [7] the neon dimer was examined, these findings of possible ICD after a one-site Auger cascade were confirmed experimentally for argon dimers first [8,9]. Further experimental work on krypton, argon, and mixed krypton and/or argon clusters showed similar results [10,11]. In the present work we investigate the neon dimer, i.e., the system originally proposed by Santra *et al.*

A compilation of the decay processes in a dimer are shown in Fig. 1. In the following those processes will be described in more detail: The matrix element of ICD is analogous to that of a standard *one-site* Auger decay (see, e.g., [1], final equation). It involves the initial, the final state, and the electron–electron-Coulomb interaction. The matrix element needs to comply with the indistinguishability of the participating electrons. Those contributions, however, lead to two different physical pictures as soon as the electrons involved are located on two different, spatially separated atoms as in the case of ICD [12,13]: in one case an electron at the initially excited atom fills up the vacancy. The energy gained from that transition is transferred to the neighboring atom which emits an electron. This energy transfer is mediated by Coulomb interaction, i.e., a virtual photon, and thus occurs due to dipole-dipole interaction with a probability that varies asymptotically with $1/R^6$ (with R being the internuclear distance of the two participating atoms) [14]. This process is termed "direct contribution" in literature [14,15] and is shown schematically in Fig. 1(2a). The second contribution consists of an electron being transferred from the neighbor-
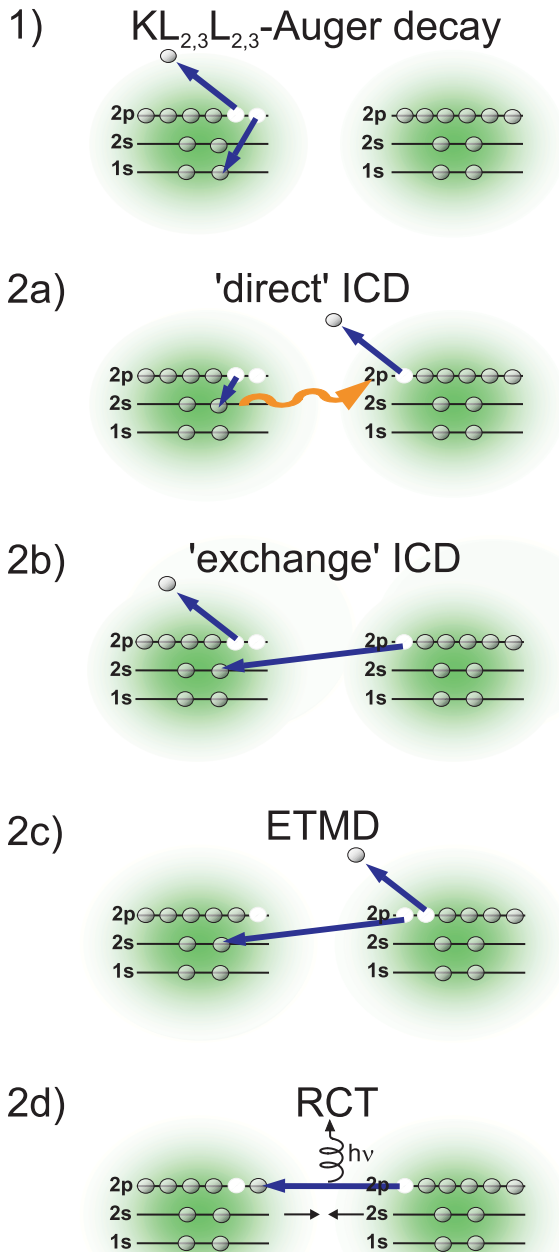
FIG. 1. (Color online) Different decay mechanisms following the 1*s* photoionization and an Auger decay in Ne$_2$. (a) The "direct" contribution of an ICD via the exchange of a virtual photon, in (b) and (c) the ICD happens via the transfer of an electron from the neutral neighbor to the inner shell vacancy leading to the emission of a valence electron from (b) the initially excited atom and (c) the neighboring atom. (d) The radiative charge transfer following the approach of both neon atoms along the attractive potential of the state Ne^{2+}/Ne.

ing atom to the vacancy leading to the emission of an ICD electron from the initially excited atom. As an electron is transferred that process is termed "exchange contribution" and, as being mainly dependent on the wave function overlap, it shows an exponential dependence on *R*, Fig. 1(2b). In principle both processes may contribute to ICD. It has been

shown, however, that they can be distinguished experimentally by examining the parity of the individual atoms of the initial state before ICD and the final state after ICD. For the direct contribution a flip in parity for the excited atoms is mandatory, as angular momentum is transferred by the virtual photon. That change in parity, however, is not required for electron transfer: therefore by examining the parity of each atom before and after the decay the direct and the exchange contributions can be distinguished, e.g., for shakeup states of different symmetry as shown in [6].

In close relation to the exchange contribution to ICD another process named "electron transfer mediated decay" (ETMD) is possible, as shown in Fig. 1(2c): in this case, just as for the exchange case, an electron is transferred from the neighbor to the initially excited atom. The energy gained from that transition is now used to emit an electron from the neighbor thus leaving a singly ionized atom (which was the one with the initial vacancy before the decay) and a doubly charged neighbor.

In many cases the potential energy surfaces of raregas dimers consisting of a neutral and a charged atom (e.g., Ne^{2+}/Ne) are attractive. Therefore, even if both particles are electronically stable another mechanism is possible. As the two atoms approach each other an electron from the neutral atom may be transferred to the charged atom, as the overall system reduces its potential energy in that process [16–18]. In order to enable this charge transfer (CT) a crossing of the corresponding initial and final state potential energy surfaces is needed. If such a crossing is not present, still that type of decay may occur: the surplus of potential energy can be emitted via a photon when dropping from the initial to the final state. This decay can be found in literature as "radiative charge transfer" (RCT) [19,20] and is depicted in Fig. 1(2d).

As already pointed out before, the different decay pathways usually have different probabilities for *R* and may depend on the symmetry of the electronic states the participating atoms are in. The electronic state can be deduced in an experiment in most cases from measuring the total energy of the system. This is achieved experimentally by detecting the kinetic energy of all fragments in coincidence. The internuclear distance can be deduced in our experimental approach, as well. By measuring the momentum of both ions from the decay in coincidence, the internuclear distance of the two atoms at the time the Coulomb explosion was triggered can be inferred from the kinetic energy of the ions [kinetic energy release (KER)].

II. EXPERIMENTAL SETUP

The measurements were performed at beamline UE56/1 SGM at the Berlin synchrotron (BESSY II) using the COLTRIMS technique [21–23]. In a COLTRIMS setup a supersonic jet is crossed with the photon beam from the synchrotron, which was used in the single bunch mode to do a time-of-flight measurement. The overlap of the two beams defines a reaction region of approximately $0.5 \times 0.5 \times 3$ mm^3. Charged particles that were produced in the photo reaction are guided by homogeneous electric and magnetic fields to two position and time sensitive microchannel plate

detectors with delay line position readout [24,25]. By measuring the time of flight and the position of impact on the detector, the initial vector momentum of each particle is obtained during offline analysis. The guiding fields (E =20V/cm and B=6 Gauss, respectively) were chosen such that electrons with an initial kinetic energy of up to 12 eV and ions with an energy of up to 10 eV are detected in coincidence with a solid angle of emission of 4π. Both the electron and the ion arm of the spectrometer incorporated a field-free drift region in order to employ Wiley-McLaren time focusing [26]. A triple coincidence condition requiring the detection of two ions and at least one electron was used during data acquisition in order to suppress events originating from monomer and residual gas ionization. During offline analysis valid events of a neon dimer breaking up after photoionization were identified by checking for momentum conservation of the two ions: as the dimer fragments in a Coulomb explosion, the ions' momenta have to be equal in magnitude and directed in opposite directions. The supersonic neon jet was precooled to 160 K. Employing a driving pressure of 7.5 bar and a nozzle with a diameter of 30 μm a maximum ratio of neon dimers in the gas jet of $\approx$1% was achieved.

III. RESULTS

The relaxation pathways following 1*s* photoionization and Auger decay in Ne_2 result in a symmetric ($Ne^{1+}+Ne^{1+}$) and an asymmetric ($Ne^{2+}+Ne^{1+}$) breakup channel, populated with an intensity ratio of about 3:1. To identify the different pathways leading to fragmentation we use Fig. 2, in which the kinetic energy of the fragment ions (KER) and the corresponding electron energy is shown for each event on a logarithmic color scale. Choosing a logarithmic representation of the data emphasizes pathways with low intensity (depicted as α_n, β_n, γ_n, and δ_n) with respect to the main channels A, B, C, D, E, and F. In Figs. 2(a) and 2(b), recorded at a photon energy of $h\nu$=880.2 eV, the photoelectrons appear at E_e=10 eV. The diagonal lines are the result of an interatomic Coulombic decay, in which the sum of the KER and the kinetic energy of the ICD electrons E_e is a constant [3].

In the next paragraph we will first describe the main decay channels A and B for the symmetric charge breakup [Fig. 2(a)], followed by the description of the main decay paths C, D, E, and F resulting in the asymmetric charge breakup of the neon dimer [Fig. 2(b)]. Subsequently the weaker decay channels α_n, β_n, γ_n, and δ_n will be identified and an estimation of the intensities of all observed decay processes is given.

IV. MAIN DECAY CHANNELS

A. Symmetric breakup channel

Even though a photon energy 10 eV above the 1*s* threshold of Ne_2 was chosen in our experiment, still, the photoionization of the 2*s* shell occurs with a probability of $\approx$3%. The 2*s* photoelectron at E_e=831.7 eV is off the scale of Fig. 2(a). The diagonal line A with a sum energy of 5.4 eV, however, results from the corresponding ICD electron just as demon-
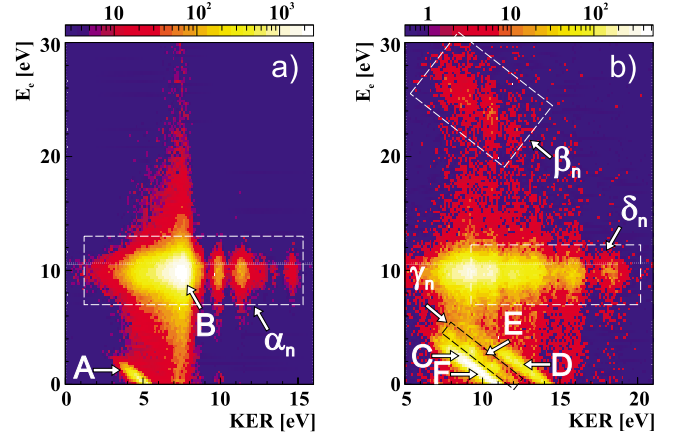
FIG. 2. (Color online) Electron energy E_e as a function of the kinetic energy release (KER) for both charge breakups, Ne^{1+} +Ne^{1+} in (a) and $Ne^{2+}+Ne^{1+}$ in (b). The intensity is shown on a logarithmic scale. With the photon energy of $h\nu$=880.2 eV the 1*s* photoelectrons have an energy of 10 eV. The diagonal lines are a clear evidence for ICD. Line A with a sum energy of 5.4 eV results from a virtual photon exchange following the 2*s* photoionization of Ne_2. Lines C, D, E, and F indicate an ICD process after the 1*s* photoionization and an Auger decay in Ne_2, where line C is produced via the virtual photon exchange yielding a sum energy of 11.1 eV. Line D with a sum energy of 14.3 eV occurs as ICD via electron transfer happens and channel E and F represent an ETMD with a sum energy of 12.4 eV and 10.8 eV, respectively. In channel B an RCT happens after 1*s* photoionization and an Auger decay. Beside these main decay channels A to F, α_n, β_n, and γ_n occur in radiationless charge transfers (CT), δ_n can be allocated to the double Auger processes. The events of channel β_n in the energy region E_e between 20 and 30 eV are detected with a solid angle of $\pm$50°.

strated in [3]. For large internuclear distances R the kinetic energy release corresponds directly to the internuclear distance at the time the two fragment ions were created. In atomic units for two singly charged ions the relation can be inferred from simple Coulomb repulsion as (KER)=1/R [27,28]. The average KER of 4.7 eV corresponds to an internuclear distance of $R\approx$3.05 Å which shows that ICD after 2*s* ionization is a fast process occurring close to the equilibrium distance R_0=3.1 Å of the neon atoms in the ground state of Ne_2. This finding is consistent with corresponding results in [6] and is in excellent agreement with the theoretical predictions [29].

The electronic decay in channel A can be described as

$$Ne/Ne + h\nu \rightarrow Ne^{1+}(2s^{-1})[^2S]/Ne + e^-_{2s,ph}$$
$$\rightarrow Ne^{1+}(2p^{-1})[^2P] + Ne^{1+}(2p^{-1})[^2P]$$
$$+ e^-_{2s,ph} + e^-_{2p,ICD}.$$
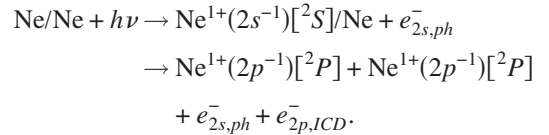
Channel B in Fig. 2(a) occurs at higher KER than the ICD identified in channel A. Its mean value of KER$\approx$7 eV corresponds to an internuclear distance R of $\approx$2 Å. Feature B is accompanied by a high-energy Auger electron of $\approx$800 eV, which is not considered here because of low detection efficiency and low-energy resolution.

To result in the symmetric charge breakup of Ne^{1+} $+Ne^{1+}$ one can think of three pathways which could describe the decay in channel B after $1s$ photoionization of the dimer,

$$Ne/Ne + h\nu \rightarrow Ne^{1+}(1s^{-1})[^2S]/Ne$$

$$(a) \rightarrow Ne^{2+}(2p^{-2})[^1D \text{ or } ^1S]/Ne + e_{Au}^-$$

$$\rightarrow Ne^{1+}(2p^{-1})[^2P] + Ne^{1+}(2p^{-1})[^2P] + e_{Au}^- + h\nu$$

$$(b) \rightarrow Ne^{2+}(2s^{-1}2p^{-1})[^3P]/Ne + e_{Au}^-$$

$$\rightarrow Ne^{1+*}(2p^{-2}nl) + Ne^{1+} + e_{Au}^-$$

$$(c) \rightarrow Ne^{1+}(2p^{-1})[^2P]/Ne^{1+}(2p^{-1})[^2P] + e_{Au}^-$$

$$\rightarrow Ne^{1+}(2p^{-1})[^2P] + Ne^{1+}(2p^{-1})[^2P] + e_{Au}^-. \quad (1)$$

Pathway (c) can be excluded because a two-site Auger decay is negligible for large internuclear distance as soon as a one-site Auger decay is energetically possible [7,30–32]. Pathway (a) and (b) are known to be populated in the initial Auger decay in a branching ratio of $\approx 10:1$ [31] so the RCT, described in (a), is by far the dominant channel. The RCT was also presented in the work of Saito *et al.* [32] as the dominant decay of the symmetric breakup of Ar_2. Pathway (b) depicting nonradiative CT will be described in Sec. V.

The relevant potential curves for pathway (a) are given in Fig. 3. The two possible initial states $Ne^{2+}(2p^{-2})[^1D$ and $^1S]/Ne$, indicated as (2) and (3), are populated in a fast Auger decay (2.5 fs) in the region of the equilibrium distance of the Ne_2 ground state and with an intensity of 7:1, respectively [31]. The Auger decay into the $Ne^{2+}(2p^{-2})[^3P]/Ne$ state is much weaker than that into the $Ne^{2+}(2p^{-2})[^1D$ and $^1S]/Ne$ states [7]. The following slow radiative decay (with a lifetime of the initial state in the ns region) allows the two neon atoms to approach along the attractive potential of the one-site dicationic state $Ne^{2+}(2p^{-2})/Ne$ before the radiative charge transfer into $Ne^{1+}(2p^{-1})[^2P]/Ne^{1+}(2p^{-1})[^2P]$ (1) takes place in the region of the potential minimum of the intermediate state [31,32]. In the repulsive final state the neon dimer then fragments in a Coulomb explosion.

Summarizing, the full decay path of channel B can be written as

$$Ne/Ne + h\nu \rightarrow Ne^{1+}(1s^{-1})[^2S]/Ne + e_{1s,ph}^-$$

$$\rightarrow Ne^{2+}(2p^{-2})[^1D \text{ or } ^1S]/Ne + e_{1s,ph}^- + e_{2p,Au}^-$$

$$\rightarrow Ne^{1+}(2p^{-1})[^2P] + Ne^{1+}(2p^{-1})[^2P] + e_{1s,ph}^-$$

$$+ e_{2p,Au}^- + h\nu.$$
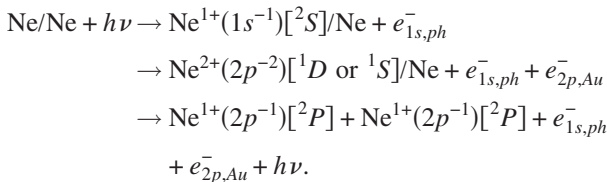
B. Asymmetric breakup channel

The diagonal lines C, D, E, and F in Fig. 2(b) form the main features in the case of an asymmetric breakup into $Ne^{2+}+Ne^{1+}$. Due to the constant sum energy $E_e+(KER)$, as indicated by the 45° diagonal, they can be identified as ICD processes which occur at different KERs, as well. Beside these diagonal lines we see for every channel the correspond-
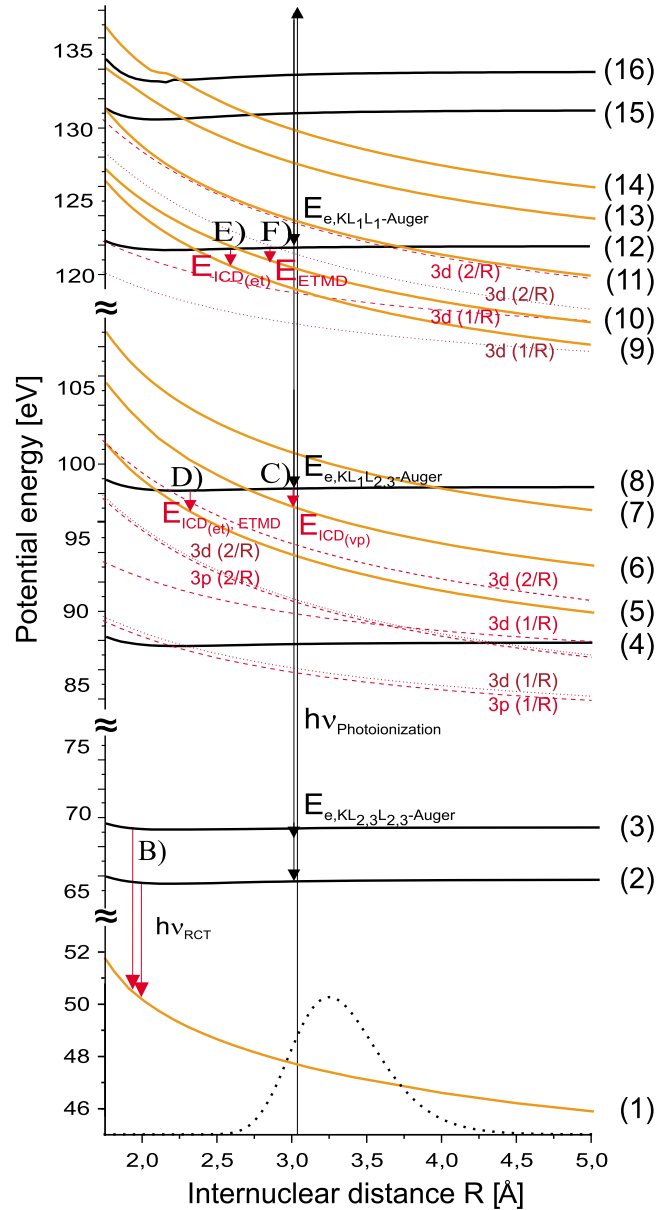
FIG. 3. (Color online) Relevant potential curves for the different decay channels happening after the $1s$ photoionization of Ne_2 [31]. The $1s$ photoionization following the Auger decay takes place around the equilibrium distance $R_0=3.1$ Å. The dotted line at the bottom of this figure describes the initial wave function. The black solid curves represent the one-site dicationic and tricationic states Ne^{2+}/Ne and Ne^{3+}/Ne generated in an Auger decay or a double Auger decay of the $1s$ vacancy. The gray (orange online) solid curves describe the two-site dicationic and tricationic states Ne^{1+}/Ne^{1+} and Ne^{2+}/Ne^{1+} populated in an RCT, ICD, or radiationless CT. The dashed and dotted lines indicate the satellite states Ne^{1+*}/Ne^{1+} being relevant to the observed decays in Ne_2. The energetically lower ones between ≈ 85 eV and ≈ 100 eV represent the potential bands of the satellite states $Ne^{1+*}(2p^{-2}[^1D]3d)/Ne^{1+}(2p^{-1})[^2P]$ (dotted lines) and $Ne^{1+*}(2p^{-2}[^1S]3d$ and $3p)/Ne^{1+}(2p^{-1})[^2P]$ (dashed lines). The higher ones between ≈ 120 eV and ≈ 130 eV describe the potential bands of $Ne^{1+*}(2p^{-2}[^1S]3d)/Ne^{1+}(2s^{-1})[^2S]$ (dotted lines) and $Ne^{1+*}(2s^{-1}2p^{-1}[^1P]3d)/Ne^{1+}(2p^{-1})[^2P]$ (dashed lines). For the assignments of states 1–16 see Fig. 5.

ing 10 eV 1s photoelectron. The high energetic Auger electron is not shown in spectrum Fig. 2(b) due to the low detection efficiency and the low resolution in this energy region.

A clear identification of the initial and the final state populated in these ICD channels is possible by determining the different sum energies KER+$E_{e,ICD}$, where the initial state is Ne^{2+}/Ne generated after Auger decay. The final state is the repulsive state of the dimer which Coulomb explodes into $Ne^{2+}+Ne^{1+}$.

In channel C the sum energy (KER)+$E_{ICD_{(vp)}}$ is equal to 11.1 eV representing the ICD from $Ne^{2+}(2s^{-1}2p^{-1})[^1P]$/Ne (8) into $Ne^{2+}(2p^{-2})[^1D]/Ne^{1+}(2p^{-1})[^2P]$ (6). The crossing of the curves at an internuclear distance of 2.6 Å corresponds to the case where $E_{ICD_{(vp)}}$ is equal to zero and the full relaxation energy of 11.1 eV is converted to the KER. The index ICD$_{(vp)}$ should make clear that this direct ICD happens via the exchange of a virtual photon as shown in Fig. 1(2a). The measured KER in channel C ranges from ≈8 to ≈11.1 eV, corresponding to an internuclear distance R of ≈3.6 Å to ≈2.6 Å. The internuclear distance R of ≈2.6 Å agrees reasonably with the crossing point of the potential curves (8) and (6) in Fig. 3 at $R=2.7$ Å. The measured mean R is close to the equilibrium distance of Ne_2 in the ground state similar to the case of ICD after 2s ionization.

Channel D with a higher sum energy (KER)+$E_{ICD_{(et)}}$ of 14.3 eV covers the range of ≈11 eV$<$KER$<$≈14.3 eV corresponding to R being ≈2.6 Å to ≈2 Å. The index ICD$_{(et)}$ represents the fact that the ICD occurring in this channel happens via an electron transfer where the same initial state as in channel C $Ne^{2+}(2s^{-1}2p^{-1})[^1P]$/Ne (8) decays into $Ne^{2+}(2p^{-2})[^3P]/Ne^{1+}(2p^{-1})[^2P]$ (5). The decay is described by an electron transfer which can be either an exchange ICD or ETMD. These two processes are schematically shown in Figs. 1(2b) and 1(2c) and cannot be distinguished in the case of channel D as they both result in the same final state $Ne^{2+}(2p^{-2})[^3P]/Ne^{1+}(2p^{-1})[^2P]$ (5). The populated potential curves of channel D are also given in Fig. 3. The fact that the exchange ICD and the ETMD occur at smaller internuclear distances (i.e., higher KER) than the direct ICD is due to their dependence on the spatial overlap of the involved wave functions [7,14,15,33]. Therefore channel D is suppressed at large internuclear distances where channel C is still open [6]. Summarizing, the decays in channel C and D were identified as

$$Ne/Ne + h\nu \rightarrow Ne^{1+}(1s^{-1})[^2S]/Ne + e^-_{1s,ph}$$
$$\rightarrow Ne^{2+}(2s^{-1}2p^{-1})[^1P]/Ne + e^-_{1s,ph} + e^-_{2p,Au}$$
$$\rightarrow Ne^{2+}(2p^{-2})[^1D] + Ne^{1+}(2p^{-1})[^2P]$$
$$+ e^-_{1s,ph} + e^-_{2p,Au} + e^-_{2p,ICD}(C)$$
$$\rightarrow Ne^{2+}(2p^{-2})[^3P] + Ne^{1+}(2p^{-1})[^2P]$$
$$+ e^-_{1s,ph} + e^-_{2p,Au} + e^-_{2p,ICD/ETMD}(D).$$
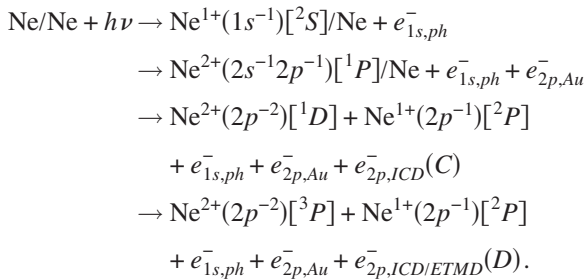
Our experimental results show a third diagonal line in the asymmetric charge breakup of Ne_2 labeled as channel E in Fig. 2. The sum energy of this ICD is 12.4 eV. The mean

KER of ≈11 eV corresponds to an internuclear distance R of ≈2.6 Å. It indicates the decay from $Ne^{2+}(2s^{-2})[^1S]$/Ne (12) into $Ne^{2+}(2s^{-1}2p^{-1})[^3P]/Ne^{1+}(2p^{-1})[^2P]$ (9) in an ICD process via an electron transfer. The potential curves being relevant to channel E are given in Fig. 3 where also a second decay F, predicted in [31], from $Ne^{2+}(2s^{-2})[^1S]$/Ne (12) is possible. Thus, in channel F the same initial state as in channel E relaxes in an ETMD process to $Ne^{2+}(2p^{-2})[^3P]/Ne^{1+}(2s^{-1})[^2S]$ (10) with a sum energy of 10.8 eV which corresponds to an internuclear distance R of ≈2.65 Å. With our total resolution of ≈0.8 eV for the electron energy this diagonal line, labeled as channel F in [Fig. 2(b)] cannot be distinguished from the diagonal line in channel C. The reactions in channel E and F were found to be:

$$Ne/Ne + h\nu \rightarrow Ne^{1+}(1s^{-1})[^2S]/Ne + e^-_{1s,ph}$$
$$\rightarrow Ne^{2+}(2s^{-2})[^1S]/Ne + e^-_{1s,ph} + e^-_{2s,Au}$$
$$\rightarrow Ne^{2+}(2s^{-1}2p^{-1})[^3P] + Ne^{1+}(2p^{-1})[^2P]$$
$$+ e^-_{1s,ph} + e^-_{2s,Au} + e^-_{2p,ICD}(E)$$
$$\rightarrow Ne^{2+}(2p^{-2})[^3P] + Ne^{1+}(2s^{-1})[^2S]$$
$$+ e^-_{1s,ph} + e^-_{2s,Au} + e^-_{2p,ETMD}(F).$$
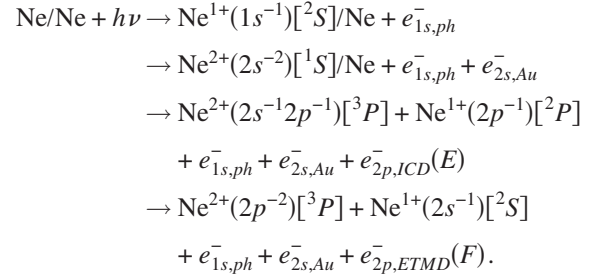
V. WEAKER DECAY CHANNELS

Beside the dominant channels A to F in the symmetric, as well, as in the asymmetric charge breakup of Ne_2 one can see in both, Figs. 2(a) and 2(b), further decay channels α_n, β_n, γ_n, and δ_n which represent about ≈10% of all relaxation processes following the 1s photoionization and the subsequent Auger decay.

The specific channels α_n which appear in the KER region between 2 and 14.5 eV corresponding to internuclear distances of $R \approx 7$ Å to ≈1 Å, can be explained by a charge transfer due to nonadiabatic coupling between $Ne^{2+}(2s^{-1}2p^{-1})[^3P]$/Ne (4) and $Ne^{1+*}(2p^{-2}[^1S]3d$ or $3p)/Ne^{1+}(2p^{-1})[^2P]$ or $Ne^{1+*}(2p^{-2}[^1D]3d)/Ne^{1+}(2p^{-1})[^2P]$ [Eq. (1)(b)]. This decay forms, with respect to the RCT depicted in Eq. (1)(a), the competing relaxation process in the symmetric charge breakup. The satellite states are calibrated in the infinity to $E_{ion}-6$ or $E_{ion}-10$ eV, whereas E_{ion} is the energy of the ionized atom and ≈6 and ≈10 eV are the ionization energies of the 3d and the 3p electron in average for both neon atoms. These radiationless CT processes were also observed in [9,34] after the $L_{2,3}M_1M_{2,3}$ Auger decay of Ar_2 and Ar_3.

A reason for the high KER region of α_n is the fact that the potential curves of the satellite states fall at close distances with $2/R$ since the highly excited Rydberg electron does not contribute to the shielding. Assuming a $2/R$ potential channel α_n appearing at a KER of 14.5 eV, corresponds to the radiationless CT due to nonadiabatic coupling in the region of $R \approx 2$ Å. By taking into account the $2/R$ potential of the satellite state $Ne^{1+*}(2p^{-2}[^1S]3d)/Ne^{1+}(2p^{-1})[^2P]$ also the crossing with $Ne^{2+}(2s^{-1}2p^{-1})[^1P]$/Ne (8) will form a small fraction of the possible CT processes explaining α_n. The potential bands of the satellite states being relevant for channel
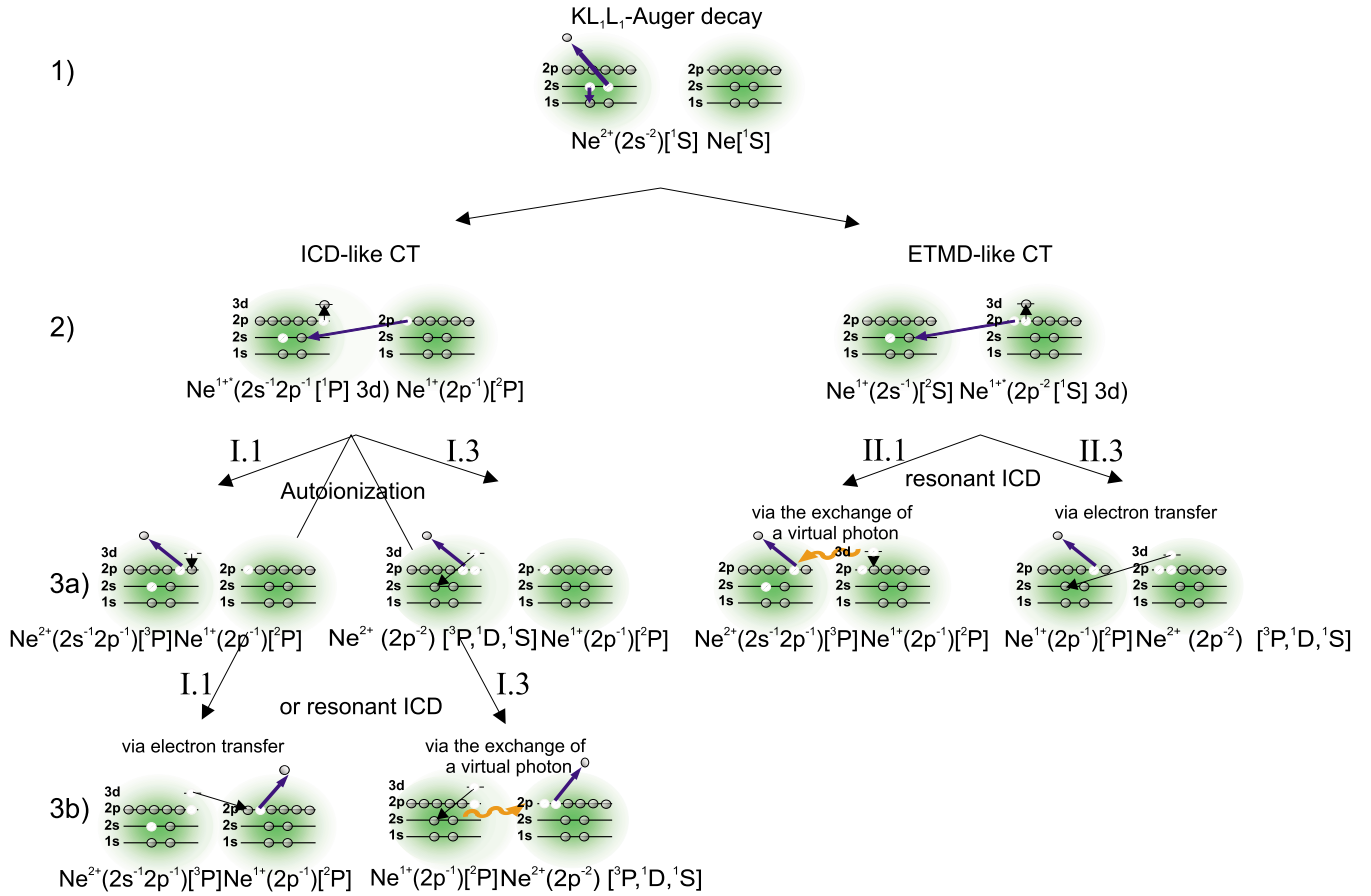
FIG. 4. (Color online) With an intensity of $\approx 4\%$ three-step decays happen after the $1s$ photoionization of Ne_2 resulting in the asymmetric breakup $Ne^{2+}+Ne^{1+}$. (1) describes the KL_1L_1-Auger decay into $Ne^{2+}(2s^{-2})[^1S]/Ne$ [indicated as (12) in Fig. 3]. (2) In an ICD-like or an ETMD-like CT the satellite state $Ne^{1+*}(2s^{-1}2p^{-1}[^1P]3d)/Ne^{1+}(2p^{-1})[^2P]$ or $Ne^{1+*}(2p^{-2}[^1S]3d)/Ne^{1+}(2s^{-1})(^2S)$ is populated. 3(a) and 3(b): An autoionization or a resonant ICD into the Coulomb-exploding final state $Ne^{2+}(2s^{-1}2p^{-1})[^3P]/Ne^{1+}(2p^{-1})[^2P]$ (9) or $Ne^{2+}(2p^{-2})[^3P, ^1D, ^1S]/Ne^{1+}(2p^{-1})[^2P]$ (5), (6), (7) is identified out of the experimental data. Two more possible decay paths, described in the text as (I.2) and (II.2), are not visible in the data, probably due to a lower intensity in comparison with the dominant overlapping channel C.

α_n are indicated as dashed lines $\{Ne^{1+*}(2p^{-2}[^1D]3d$ and $3p)/Ne^{1+}(2p^{-1})[^2P]\}$ and dotted lines $\{Ne^{1+*}(2p^{-2}[^1D]3d)/Ne^{1+}(2p^{-1})[^2P]\}$ in the energy region between ≈ 85 and ≈ 100 eV in Fig. 3.

The channels β_n and γ_n at a KER of ≈ 8, ≈ 9.5, ≈ 10.5, and ≈ 12 eV, corresponding to R of ≈ 3.6, ≈ 3.0, ≈ 2.7, and ≈ 2.4 Å, could be explained by a three-step-decay process in which an ICD-like or an ETMD-like CT due to a nonadiabatic coupling between the initial state of channel E and F, $Ne^{2+}(2s^{-2})[^1S]/Ne$ (12), and the satellite states $Ne^{1+*}(2s^{-1}2p^{-1}[^1P]3d)/Ne^{1+}(2p^{-1})[^2P]$ and $Ne^{1+*}(2p^{-2}[^1S]3d)/Ne^{1+}(2s^{-1})[^2S]$ happens before the two-site tricationic state Ne^{2+}/Ne^{1+} is populated in an autoionization or a resonant ICD process. The potential bands of theses satellite states, bound by the upper $2/R$ and the lower $1/R$ potential curve of the satellite states, are indicated in Fig. 3 as dashed lines $\{Ne^{1+*}(2s^{-1}2p^{-1}[^1P]3d)/Ne^{1+}(2p^{-1})[^2P]\}$ and dotted lines $\{Ne^{1+*}(2p^{-2}[^1S]3d)/Ne^{1+}(2s^{-1})[^2S]\}$ between ≈ 120 and ≈ 130 eV.

The possible autoionization [35,36] and resonant ICD processes [4,5] of both satellite states will be described in the following. Beginning with the decay of the satellite state $Ne^{1+*}(2s^{-1}2p^{-1}[^1P]3d)/Ne^{1+}(2p^{-1})[^2P]$ populated in an ICD-like CT the possible pathways are as follows:

(I.1) Autoionization or resonant ICD via an electron transfer ($RICD_{(et)}$) into $Ne^{2+}(2p^{-1}2p^{-1})[^3P]/Ne^{1+}(2p^{-1})[^2P]$ (9)

(I.2) $RICD_{(vp)}$ into $Ne^{2+}(2p^{-2})[^3P]/Ne^{1+}(2s^{-1})[^2S]$ (10).

(I.3) Autoionization or $RICD_{(vp)}$ into $Ne^{2+}(2p^{-2})[^3P, ^1D,$ or $^1S]/Ne^{1+}(2p^{-1})[^2P]$ (5),(6),(7).

The possible processes following the population of the satellite state $Ne^{1+*}(2p^{-2}[^1S]3d)/Ne^{1+}(2s^{-1})[^2S]$ in an ETMD-like charge transfer are as follows:

(II.1) $RICD_{(vp)}$ into $Ne^{2+}(2s^{-1}2p^{-1})[^3P]/Ne^{1+}(2p^{-1})[^2P]$ (9).

(II.2) Autoionization into $Ne^{2+}(2p^{-2})[^3P]/Ne^{1+}(2s^{-1})[^2S]$ (10).

(II.3) ($RICD_{(et)}$) into $Ne^{2+}(2p^{-2})[^3P, ^1D,$ or $^1S]/Ne^{1+}(2p^{-1})[^2P]$ (5),(6),(7).

Pathways (I.1) and (II.1) are clearly visible in the experimental data. They can be identified by the islands γ_n along the diagonal line from channel E. Pathways (I.3) and (II.3) are responsible for the islands β_n in the energy region $E_e \approx 20$ to ≈ 30 eV, whereas the resolution is not enough to

initial state → (energy at R = 3.1 A) / final state ↓ (energy in fragmented state)	$Ne^{2+}(2p^{-2})[^1S,^1D]/Ne$ (2),(3)	$Ne^{2+}(2s^{-1}2p^{-1})[^3P]/Ne$ (4)	$Ne^{2+}(2s^{-1}2p^{-1})[^1P]/Ne$ (8)	$Ne^{2+}(2s^{-2})[^1S]/Ne$ (12)	$Ne^{3+}(2p^{-3})[^2D,^2P]/Ne$ (15),(16)
$Ne^{1+}(2p^{-1})[^2P]$ + $Ne^{1+}(2p^{-1})[^2P]$　(1)	RCT (B) [≈67.5 %]				
$Ne^{1+*}(2p^{-2}nl)[^1S]$ + $Ne^{1+}(2p^{-1})[^2P]$　(*)		CT (α_n) [≈7.5 %]			
$Ne^{2+}(2p^{-2})[^3P]$ + $Ne^{1+}(2p^{-1})[^2P]$　(5)			ICD(et), ETMD (D) [≈4.5 %]		
$Ne^{2+}(2p^{-2})[^1D]$ + $Ne^{1+}(2p^{-1})[^2P]$　(6)			ICD(vp) (C) [≈13.5 %]		
$Ne^{2+}(2p^{-2})[^3P,^1D,^1S]$ + $Ne^{1+}(2p^{-1})[^2P]$　(5),(6),(7)				3-step-decay (β_n) [< 4 %]	
$Ne^{2+}(2s^{-1}p^{-1})[^3P]$ + $Ne^{1+}(2p^{-1})[^2P]$　(9)				a) ICD(et) (E) [≈ 3.5 %] b) 3-step-decay (γ_n) [< 4 %]	
$Ne^{2+}(2p^{-2})[^3P]$ + $Ne^{1+}(2s^{-1})[^2S]$　(10)				ETMD (F) [≈ 2.5 %]	
$Ne^{2+}(2p^{-2})[^1D]$ + $Ne^{1+}(2s^{-1})[^2S]$　(11)					CT (δ_n) [≈ 1 %]
$Ne^{2+}(2p^{-2})[^1S]$ + $Ne^{1+}(2s^{-1})[^2S]$　(13)					
$Ne^{2+}(2s^{-1}2p^{-1})[^1P]$ + $Ne^{1+}(2p^{-1})[^2P]$　(14)					

FIG. 5. Different decay channels from the one-site dicationic initial state, generated in an Auger decay following the 1s photoionization of Ne_2 into the two-site charged final state in which both neon ions are emitted under 180° in a Coulomb explosion. In squared brackets the estimated intensity of the different decay channels following the 1s photoionization of Ne_2 are given. ((*) The satellite states relevant to the observed decays α_n in Ne_2 cover the energy region between 85 and 100 eV in Fig. 3.

FIG. 6. Kinetic energy distribution of the ICD electrons emitted in (I) channel C ("direct" ICD), (II) channel D ("exchange ICD") and (III) channel E (ETMD). For the different ICD processes occurring in channel C, D, and E, see Fig. 1 as a reference. In all cases the electron energy is calculated out of the KER due to the better energy resolution of the ions. Due to the lack of resolution an integration over the whole region of channel C and F is done in (I), whereas the fraction of channel F is ≈16% of channel C. In (III) one can see the overlying island structure of channel γ_n.

resolve the final state $Ne^{2+}(2p^{-2})[^3P, ^1D$, or $^1S]/$ $Ne^{1+}(2p^{-1})[^2P]$ (5),(6), or (7). However, in the experimental data pathways (I.2) and (II.2) are not visible due to much lower intensity in comparison with the dominant overlapping channel C. The observed three-step decays of $Ne^{2+}(2s^{-2})[^1S]/Ne$ (12) described in pathways (I.1), (I.3), (II.1), and (II.3) are schematically shown in Fig. 4.

A three-step decay of the 1s vacancy in Ne_2 can also contribute to the symmetric charge breakup of Ne_2. The repulsive satellite states populated in channel β_n and γ_n can also dissociate into $Ne^{1+*}+Ne^{1+}$ instead of undergoing an autoionization or a resonant ICD process. This will lead to the low KER region in channel α_n: as mentioned above the satellite states are populated at internuclear distances of R between ≈3.6 and ≈2.4 Å. In the case of dissociation into $Ne^{1+*}+Ne^{1+}$ this region of R is converted to a KER between 4 and 6 eV and with this it could explain the 1s photoelectrons in the low KER region of α_n in the symmetric charge breakup of Ne_2.

To explain the appearance of δ_n in the asymmetric breakup one has to take into account that a double Auger process can happen after the 1s photoionization of Ne_2 with a probability of ≈3% [37–40]. By looking at the potential curves in Fig. 3 one can describe channel δ_n as a radiationless CT due to nonadiabatic coupling between $Ne^{3+}(2p^{-3})[^2P]/Ne$ (16) or $Ne^{3+}(2p^{-3})[^2D]/Ne$ (15) generated in a double Auger decay and the two-site tricationic states $Ne^{2+}(2s^{-1}2p^{-1})[^1P]/Ne^{1+}(2p^{-1})[^2P]$ (14), $Ne^{2+}(2p^{-2})[^1S]/Ne^{1+}(2s^{-1})[^2S]$ (13), and $Ne^{2+}(2p^{-2})[^1D]/$ $Ne^{1+}(2s^{-1})[^2S]$ (11). Figure 3 shows crossings of theses states at internuclear distances of 2.7 Å, 2.2 Å, and 1.8 Å. This is in agreement with the structure in channel δ_n appearing at a KER of 10.5 eV, 13 eV, and 16 eV, whereas δ_n at 10.5 eV is masked by the 1s photoelectron from channel E which appears at a KER of 11 eV. While there are two possible crossings explaining the KER of 13 eV, the distribution at 18.5 eV according to a internuclear distance of ≈1.6 Å cannot be related to any of them, and until now we have no explanation for it. All decay channels occurring after the 1s photoionization following the Auger decay in Ne_2 as well as their ratios are listed in Fig. 5, whereas channel A describing the 2s photoionization of Ne_2 was not taken into account.

Considering the Auger decay rates given in [31] for the population of the initial state listed in Fig. 5, channel B takes place with a possibility of 67.5%, and 7.5% can be allocated to channel α_n. The diagonal lines of channel D and E are clearly distinguishable so that their rates of 4.5% and 3.5%, respectively can directly obtained out of Fig. 2(b). To receive

the rates for channel C and F, which cannot be separated with our resolution, again the theoretical Auger rates for the population of the initial state given in [31] were used. Therewith one can estimate a rate of 13.5% for channel C and 2.5% for channel F. However in channel C to F a small fraction of these estimated rates has to be allocated to the three-step decays (channel β_n and γ_n), described in pathway (I.1) to (I.3) and (II.1) to (II.3). These decays result in one of the final states of channel C to F and occur altogether with an intensity of $\approx 4\%$. The rates for channel δ_n cannot be estimated directly out of Fig. 2(b) because of the overlying main channels C to F. In [38] a calculated $KL_{2,3}L_{2,3}L_{2,3}$ double Auger rate of 1.64% is obtained. This is consistent with a rate of $\approx 1\%$ that we obtain for δ_n in our experiment by summing up the branching ratios of all other channels of the asymmetric breakup and comparing it to the total rate of that breakup.

In Figs. 6(I), 6(II), and 6(III) the kinetic energy distribution of the ICD electrons emitted in the decay channels C, D, and E are shown. In all three cases the kinetic energy covers the range between 0 and ≈ 4.5 eV. In channel C and D, showing the kinetic energy of a direct ICD electron and of an exchange ICD electron one can see a maximum of the distribution around ≈ 2 eV. In the electron energy distribution of channel E, in which the emitted electron also results from

an exchange ICD process, the additional structure of channel γ_n is visible.

VI. SUMMARY

In conclusion, we employed cold target recoil ion momentum spectroscopy to investigate the decay of Ne_2 after $1s$ photoionization in great detail. Multiple decay pathways were identified leading to doubly or triply charged neon dimers. Decays consisting of one-site atomic Auger decay followed by direct ICD, exchange ICD, ETMD and radiative and nonradiative charge transfer were found.

[1] L. S. Cederbaum, J. Zobeley, and F. Tarantelli, Phys. Rev. Lett. **79**, 4778 (1997).

[2] S. Marburger, O. Kugeler, U. Hergenhahn, and T. Möller, Phys. Rev. Lett. **90**, 203401 (2003).

[3] T. Jahnke, A. Czasch, M. S. Schöffler, S. Schössler, A. Knapp, M. Käsz, J. Titze, C. Wimmer, K. Kreidi, R. E. Grisenti, A. Staudte, O. Jagutzki, U. Hergenhahn, H. Schmidt-Böcking, and R. Dörner, Phys. Rev. Lett. **93**, 163401 (2004).

[4] S. Barth, S. Joshi, S. Marburger, V. Ulrich, A. Lindblad, G. Öhrwall, O. Björneholm, and U. Hergenhahn, J. Chem. Phys. **122**, 241102 (2005).

[5] T. Aoto, K. Ito, Y. Hikosaka, E. Shigemasa, F. Penent, and P. Lablanquie, Phys. Rev. Lett. **97**, 243401 (2006).

[6] T. Jahnke, A. Czasch, M. Schöffler, S. Schössler, M. Käsz, J. Titze, K. Kreidi, R. E. Grisenti, A. Staudte, O. Jagutzki, L. Ph. H. Schmidt, Th. Weber, H. Schmidt-Böcking, K. Ueda, and R. Dörner, Phys. Rev. Lett. **99**, 153401 (2007).

[7] R. Santra and L. S. Cederbaum, Phys. Rev. Lett. **90**, 153401 (2003); **94**, 199901(E) (2005).

[8] Y. Morishita, X.-J. Liu, N. Saito, T. Lischke, M. Kato, G. Prümper, M. Oura, H. Yamaoka, Y. Tamenori, I. H. Suzuki, and K. Ueda, Phys. Rev. Lett. **96**, 243402 (2006).

[9] K. Ueda, X.-J. Liu, G. Prümper, H. Fukuzawa, Y. Morishita, and N. Saito, J. Electron Spectrosc. Relat. Phenom. **155**, 113 (2007).

[10] Y. Morishita, N. Saito, I. H. Suzuki, H. Fukuzawa, X.-J. Liu, K. Sakai, G. Prümper, K. Ueda, H. Iwayama, K. Nagaya, M. Yao, K. Kreidi, M. Schöffler, T. Jahnke, S. Schössler, R. Dörner, T. Weber, J. Harries, and Y. Tamenori, J. Phys. B **41**, 025101 (2008).

[11] K. Ueda, H. Fukuzawa, X.-J. Liu, K. Sakai, G. Prüemper, Y. Morishita, N. Saito, I. H. Suzuki, K. Nagaya, H. Iwayama, M. Yao, K. Kreidi, M. Schöffler, T. Jahnke, S. Schössler, R. Dörner, T. Weber, J. Harries, and Y. Tamenori, J. Electron Spectrosc. Relat. Phenom. (to be published).

[12] K. Kreidi, T. Jahnke, Th. Weber, T. Havermeier, R. E. Grisenti, X. Liu, Y. Morisita, S. Schössler, L. Ph. H. Schmidt, M. Schöffler, M. Odenweller, N. Neumann, L. Foucar, J. Titze, B. Ulrich, F. Sturm, C. Stuck, R. Wallauer, S. Voss, I. Lauter, H. K. Kim, M. Rudloff, H. Fukuzawa, G. Prümper, N. Saito, K. Ueda, A. Czasch, O. Jagutzki, H. Schmidt-Böcking, S. K. Semenov, N. A. Cherepkov, and R. Dörner, J. Phys. B **41**, 101002 (2008).

[13] M. Yamazaki, J. I. Adachi, Y. Kimura, A. Yagishita, M. Stener, P. Decleva, N. Kosugi, H. Iwayama, K. Nagaya, and M. Yao, Phys. Rev. Lett. **101**, 043004 (2008).

[14] V. Averbukh, I. B. Müller, and L. S. Cederbaum, Phys. Rev. Lett. **93**, 263002 (2004).

[15] R. Santra, J. Zobeley, and L. S. Cederbaum, Phys. Rev. B **64**, 245104 (2001).

[16] R. Johnsen, M. T. Leu, and M. Biondi, Phys. Rev. A **8**, 1808 (1973).

[17] W. B. Maier and B. Stewart, J. Chem. Phys. **68**, 4228 (1978).

[18] D. Smith, N. G. Adams, E. Alge, H. Villinger, and W. Lindinger, J. Phys. B **13**, 2787 (1980).

[19] R. Johnsen and M. A. Biondi, Phys. Rev. A **18**, 996 (1978).

[20] J. S. Cohen and J. N. Bardsley, Phys. Rev. A **18**, 1004 (1978).

[21] R. Dörner, V. Mergel, O. Jagutzki, L. Spielberger, J. Ullrich, R. Moshammer, and H. Schmidt-Böcking, Phys. Rep. **330**, 96 (2000).

[22] J. Ullrich, R. Moshammer, A. Dorn, R. Dörner, L. Ph. Schmidt, and H. Schmidt-Böcking, Rep. Prog. Phys. **66**, 1463 (2003).

[23] T. Jahnke, Th. Weber, T. Osipov, A. L. Landers, O. Jagutzki, L. Ph. H. Schmidt, C. L. Cocke, M. H. Prior, H. Schmidt-Böcking, and R. Dörner, J. Electron Spectrosc. Relat. Phenom. **141**, 229 (2004).

[24] O. Jagutzki, V. Mergel, K. Ullmann-Pfleger, L. Spielberger, U. Spillmann, R. Dörner, and H. Schmidt-Böcking, Nucl. Instrum. Methods Phys. Res. A **477**, 244 (2002).

[25] See www.Roentdek.com for details of the detectors.

[26] W. C. Wiley and I. H. McLaren, Rev. Sci. Instrum. **26**, 1150 (1955).

[27] Th. Weber, A. O. Czasch, O. Jagutzki, A. K. Müller, V. Mergel, A. Kheifets, E. Rotenberg, G. Meigs, M. H. Prior, S. Daveau, A. Landers, C. L. Cocke, T. Osipov, R. Diez Muino, H. Schmidt-Böcking, and R. Dörner, Nature (London) **431**, 437 (2004).

[28] M. Schöffler, K. Kreidi, D. Akoury, T. Jahnke, A. Staudte, N. Neumann, J. Titze, L. Ph. H. Schmidt, A. Czasch, O. Jagutzki, R. A. Costa Fraga, R. E. Grisenti, M. Smolarski, P. Ranitovic, C. L. Cocke, T. Osipov, H. Adaniya, S. Lee, J. C. Thompson, M. H. Prior, A. Belkacem, Th. Weber, A. Landers, H. Schmidt-Böcking, and R. Dörner, Phys. Rev. A **78**, 013414 (2008).

[29] S. Scheit, V. Averbukh, H.-D. Meyer, N. Moiseyev, R. Santra, T. Sommerfeld, J. Zobeley, and L. Cederbaum, J. Chem. Phys. **121**, 8393 (2004).

[30] Ph. V. Demekhin, S. Scheit, S. D. Stoychev, and L. S. Cederbaum, preceding paper, Phys. Rev. A **78**, 043421 (2008).

[31] S. D. Stoychev, A. I. Kuleff, F. Tarantelli, and L. S. Cederbaum, J. Chem. Phys. **129**, 074307 (2008).

[32] N. Saito, Y. Morishita, I. H. Suzuki, S. D. Stoychev, A. I. Kuleff, L. S. Cederbaum, X.-J. Liu, H. Fukuzawa, G. Prümper, and K. Ueda, Chem. Phys. Lett. **441**, 16 (2007).

[33] J. Zobeley, R. Santra, and L. S. Cederbaum, J. Chem. Phys. **115**, 5076 (2001).

[34] X.-J. Liu, N. Saito, H. Fukuzawa, Y. Morishita, S. Stoychev, A. Kuleff, I. H. Suzuki, Y. Tamenori, R. Richter, G. Prümper, and K. Ueda, J. Phys. B **40**, F1 (2006).

[35] U. Becker, R. Wehlitz, O. Hemmers, B. Langer, and A. Menzel, Phys. Rev. Lett. **63**, 1054 (1989).

[36] T. Kaneyasu, Y. Hikosaka, E. Shigemasa, F. Penent, P. Lablanquie, T. Aoto, and K. Ito, J. Phys. B **40**, 4047 (2007).

[37] T. A. Carlson and M. O. Krause, Phys. Rev. Lett. **14**, 390 (1965).

[38] B. Kanngiesser, M. Jainz, S. Brünken, W. Benten, Ch. Gerth, K. Godehusen, K. Tiedtke, P. van Kampen, A. Tutay, P. Zimmermann, V. F. Demekhin, and A. G. Kochur, Phys. Rev. A **62**, 014702 (2000).

[39] J. Viefhaus, A. N. Grum-Grzhimailo, N. M. Kabachnik, and U. Becker, J. Electron Spectrosc. Relat. Phenom. **141**, 121 (2004).

[40] Y. Hikosaka, T. Aoto, P. Lablanquie, F. Penent, E. Shigemasa, and K. Ito, J. Phys. B **39**, 3457 (2006).